Published in final edited form as:
Cell Metab. 2013 February 5; 17(2): 249–260. doi:10.1016/j.cmet.2013.01.002.

Tmem64 modulates calcium signaling during RANKL-mediated osteoclast differentiation

Hyunsoo Kim[1,8], **Taesoo Kim**[2,8], **Byung-Chul Jeong**[1,3,8], **Il-Taeg Cho**[1], **Daehee Han**[1], **Noriko Takegahara**[1], **Takako Negishi-Koga**[4], **Hiroshi Takayanagi**[4], **Jae Hee Lee**[5], **Jai-Yoon Sul**[5], **Vikram Prasad**[6], **Seoung-Hoon Lee**[7], and **Yongwon Choi**[1,*]

[1]Departments of Pathology and Laboratory Medicine, University of Pennsylvania Perelman School of Medicine, Philadelphia, PA 19104, USA

[2]TKM-Based Herbal Drug Research Group, Korea Institute of Oriental Medicine, Daejeon 305-811, Korea

[3]Department of Pharmacology and Dental Therapeutics, School of Dentistry, Chonnam National University, Gwangju 500-757, Korea

[4]Department of Cell Signaling, Tokyo Medical and Dental University, Tokyo 113-8549, Japan

[5]Department of Pharmacology, University of Pennsylvania Perelman School of Medicine, Philadelphia, PA 19104, USA

[6]Department of Molecular Genetics, Biochemistry and Microbiology, University of Cincinnati College of Medicine, Cincinnati, OH 45267, USA

[7]Departments of Oral Microbiology and Immunology, Wonkwang University, School of Dentistry, Iksan 570-749, Korea

SUMMARY

Osteoclast maturation and function primarily depend on receptor activator of NF-κB ligand (RANKL)-mediated induction of nuclear factor of activated T cells c1 (NFATc1), which is further activated via increased intracellular calcium ($[Ca^{2+}]_i$) oscillation. However, the coordination mechanism that mediates Ca^{2+} oscillation during osteoclastogenesis remains ill defined. Here, we identified transmembrane protein 64 (*Tmem64*) as a regulator of Ca^{2+} oscillation during osteoclastogenesis. We found that Tmem64-deficient mice exhibit increased bone mass due in part to impaired osteoclast formation. Using in vitro osteoclast culture systems, we show here that Tmem64 interacts with sarcoplasmic endoplasmic reticulum Ca^{2+} ATPase 2 (SERCA2) and modulates its activity. Consequently, Tmem64 deficiency significantly diminishes RANKL-induced $[Ca^{2+}]_i$ oscillation, which results in reduced Ca^{2+}/calmodulin-dependent protein kinases (CaMK) IV and mitochondrial ROS, both of which contribute to achieving the CREB activity necessary for osteoclast formation. These data demonstrate that Tmem64 is a positive modulator of osteoclast differentiation via SERCA2-dependent Ca^{2+} signaling.

*Correspondence: ychoi3@mail.med.upenn.edu.
[8]These authors contributed equally to this work

Supplementary Information

Supplemental Information includes 6 figures, 1 table, and Supplemental Experimental Procedures and can be found with this article online at doi:

INTRODUCTION

Skeletal bone is maintained via continuous bone formation and destruction mediated by osteoblasts and osteoclasts (Zaidi, 2007; Zelzer and Olsen, 2003). Imbalance of bone homeostasis causes various skeletal disorders (Teitelbaum and Ross, 2003). Congenital defects in the development and function of osteoclasts lead to osteopetrosis, which is characterized by high bone mineral density. In contrast, excessive osteoclast differentiation and activity causes osteoporosis, or low bone mineral density. Therefore, investigations of osteoclast differentiation and function aim to reveal the physiology and pathology of the skeletal system and to provide a molecular basis for designing therapeutic strategies for bone remodeling diseases (Karsenty and Wagner, 2002).

Since the discovery of RANKL as an essential osteoclast differentiation factor, many of the signaling pathways required for RANKL-induced osteoclast differentiation have been identified (Walsh et al., 2006). Binding of RANKL to RANK triggers TRAF6-dependent signaling, activating NF-κB, Akt and MAP kinases (ERK, JNK and p38). In other pathways, immunoreceptor tyrosine-based activation motif (ITAM)-bearing adaptors, Fc receptor common γ subunit (FcRγ) and DNAX-activating protein 12 (DAP12) deliver co-stimulatory signals through activation of PLCγ. Activated PLCγ leads to the generation of inositol-1,4,5-triphosphate (IP_3), which mobilizes Ca^{2+} from the ER stores through inositol triphosphate receptors (IP_3Rs) (Ferron et al., 2011; Kim et al., 2002; Koga et al., 2004; Kuroda et al., 2008), and subsequently generates Ca^{2+} oscillation, which is critical for the activation of CaMKIV and NFATc1. This RANKL-induced Ca^{2+} oscillation activates Ca^{2+}/calmodulin-dependent protein kinases (CaMK)IV, followed by cAMP-responsive element binding protein (CREB) activation (Sato et al., 2006), which is also induced by mitochondrial reactive oxygen species (ROS) (Ishii et al., 2009). The CaMKIV/CREB/NFATc1 pathway is critical to osteoclast differentiation and function (Negishi-Koga and Takayanagi, 2009). Although Ca^{2+} oscillations are important triggers for efficient activation of NFATc1, the intra- and/or extracellular pathways that regulate Ca^{2+} oscillations during osteoclast differentiation are less well understood.

Sarco/endoplasmic reticulum Ca^{2+}-ATPases (SERCAs) are a family of proteins reported to be involved in Ca^{2+} homeostasis in a broad range of cells (Feske, 2007; Fu et al., 2011). SERCA proteins are encoded by a multigenic family that includes SERCA1–3 (*Atp2a1–3*). Each gene encodes at least 5 splicing isoforms. SERCA1a and SERCA1b are mainly expressed in adult and neonatal fast-twitch skeletal muscles, whereas SERCA2a is expressed in cardiac muscle. SERCA2b, which has a C-terminal extension, is ubiquitously expressed in smooth muscle tissues and non-muscle tissues, including neurons. SERCA3 also has various 3′-end splice variants and limited expression in non-muscle tissues (Dally et al., 2006). Recent studies have revealed that a number of proteins, such as ER protein 57 (also known as 1,25-MARRS, ERp57, ERp60, GRP58, or Pdia3) (Li and Camacho, 2004), calreticulin (John et al., 1998), sarcalumenin (Shimura et al., 2008), histidine-rich Ca^{2+}-binding protein (HRC) (Arvanitis et al., 2007), and calumenin (Sahoo et al., 2009), associate with and regulate SERCA2b stability and activity, but the mechanisms are not completely understood. It has recently been reported that SERCA2 heterozygosity (*SERCA2*$^{+/-}$) causes defects in osteoclast differentiation because of suppressed RANKL-induced $[Ca^{2+}]_i$ oscillations, and is associated with bone abnormalities (Yang et al., 2009).

In this study, we report that the Tmem64 is a regulator for RANKL-mediated Ca^{2+} signaling pathways via its direct association with SERCA2, which is critical for the RANKL-induced CREB activation and mitochondrial ROS generation necessary for proper osteoclast generation.

RESULTS

Tmem64 deletion increases bone mass in mice

We have previously reported that ablation of the d2 isoform of vacuolar (H^+) ATPase (v-ATPase) V0 domain (*Atp6v0d2*) in mice produces osteopetrotic bone morphogenesis due to impaired osteoclast fusion and enhanced bone formation (Lee et al., 2006). To understand the molecular bases of *Atp6v0d2*$^{-/-}$ osteoclast defects, we analyzed gene expression in wild-type (WT) and *Atp6v0d2*$^{-/-}$ osteoclast precursors using global mRNA profiles. Surprisingly, we found that only one gene, transmembrane protein 64 (Tmem64), exhibited markedly increased expression in RANKL-stimulated *Atp6v0d2*-deficient osteoclast precursors. *Tmem64* mRNA is detected in various tissues (Figure S1A), its expression is up-regulated during RANKL-induced osteoclastogenesis in vitro, and siRNA knock-down of Tmem64 inhibited osteoclast formation (Figure S1B). These findings suggest that increased *Tmem64* expression in *Atp6v0d2*$^{-/-}$ BMMs is not likely responsible for defects in *Atp6v0d2*$^{-/-}$ osteoclasts, and that *Tmem64* expression may not be regulated directly by *Atp6v0d2*. While this result disinclined further examination of an explicit relationship between *Tmem64* and *Atp6v0d2*, we believed the unique expression profile and siRNA effects of *Tmem64* merited additional examination with respect to potential function(s) in the context of osteoclast biology.

To identify the in vivo function of *Tmem64* in bone remodeling, we generated *Tmem64* knockout mice using embryonic stem (ES) cells with a disruption of the *Tmem64* gene (Figure 1A, left panel). Specific deletion of *Tmem64* genomic DNA was confirmed by Southern blotting (Figure 1A, middle panel) and sequencing; mouse genotypes were verified by PCR (Figure 1A, right panel) and sequencing analysis (data not shown). Eight weeks after birth, *Tmem64*$^{-/-}$ mice showed normal appearance and growth, and most tissues exhibited no differences between groups. However, bone microstructure imaging by high-resolution microcomputed tomography (μCT) of *Tmem64*$^{-/-}$ mice revealed significantly increased bone mass, characterized by augmented bone indices including bone mineral density (BMD), bone mineral content (BMC), trabecular bone volume per tissue volume (BV/TV), trabecular thickness (Tb.Th) and trabecular number (Tb.N), with concomitant decrease in trabecular spacing (Tb.Sp) (Figure 1B). Increased bone volume was observed starting at 6 weeks of age (Figure S1C). Bone sections with von Kossa staining also showed increased trabecular bone surface in *Tmem64*$^{-/-}$ versus WT mice (Figure 1C, left panel). Tartrate-resistant acidic phosphatase (TRAP)-stained bone sections exhibited a reduction in osteoclast numbers and osteoclast surface size in *Tmem64*$^{-/-}$ versus WT (Figure 1C, right panel). Serum TRACP-5b, an early marker of osteoclast formation, was consistently reduced in mutant mice (Figure 1D). Along with reduced in vitro osteoclast formation by *Tmem64* knockdown (Figure S1B), these results suggested a potential link between Tmem64 ablation and an intrinsic defect in osteoclast differentiation. By contrast, *Tmem64*$^{-/-}$ mice showed marked increases in osteoblast surface area, bone formation rates (Figures 1C and E), and serum osteocalcin (Figure 1F). Tmem64 expression is downregulated during osteoblast differentiation (Figure S2A). In vitro osteogenic differentiation increased in *Tmem64*$^{-/-}$ calvaria-derived osteoblast precursors versus WT, as verified by increased activity of alkaline phosphatase (ALP) and visualized by alizarin red staining for mineralized nodule formation and calcium deposits (Figure S2B). This was also confirmed by upregulation of osteoblast marker genes, such as *ALP*, collagen type I (*Col1a*), osteocalcin (*OCN*), Runx2, osterix (*Osx*), osteoprotegrin (*Tnfrsf11b)*, colony stimulating factor 1 (*Csf1*) and RANKL (*Tnfsf11*), and by enhanced activity of β-catenin in *Tmem64*$^{-/-}$ osteoblasts (as assessed by crossing to the BAT-GAL β-catenin reporter mouse) (Figures S2C and S2D). We have thus obtained strong genetic evidence, using *Tmem64*$^{-/-}$ mice, that *Tmem64* is a regulator of bone metabolism; its absence results in reduced osteoclast numbers and increased bone formation in vivo. Although *Tmem64* appears to affect both osteoclasts and osteoblasts, we

have initially focused on dissecting the role of *Tmem64* in osteoclast differentiation because we currently have a better understanding of the molecular pathways controlled by RANKL stimulation (and its attendant effects) when using a relatively homogenous population of bone marrow (BM)-derived osteoclast precursor cells.

Tmem64 positively regulates osteoclast differentiation

Our analysis of *Tmem64*$^{-/-}$ versus WT bones clearly showed reduced osteoclast numbers in vivo. Preliminary data for *Tmem64* siRNA suggested that *Tmem64* knockdown reduced RANKL-induced osteoclast generation. However, osteoclast defects in *Tmem64*$^{-/-}$ mice may have been due to cross-talk with abnormal *Tmem64*$^{-/-}$ osteoblasts. Therefore, it was necessary to determine (i) whether there were cell-intrinsic defects in the absence of *Tmem64* during RANKL-induced osteoclast generation, and (ii) at which stage(s) of osteoclast differentiation *Tmem64*$^{-/-}$ defects manifest. To determine the intrinsic cellular role of *Tmem64* in osteoclast generation, we employed a standard in vitro osteoclast culture method using M-CSF and RANKL: bone marrow macrophages (BMMs) were generated by culturing BM cells with M-CSF only and *Tmem64* knockout reconfirmed by northern blot analysis (Figure 2A, left panel); then, BMMs were induced to differentiate into osteoclasts by RANKL. When purified BM cells were induced to become osteoclasts, Tmem64 mRNA levels increased (Figure 2A, right panel; real-time PCR and RT-PCR), and *Tmem64*$^{-/-}$ BMMs stimulated with RANKL exhibited significantly fewer TRAP^{+} multinucleated cells (MNCs), considered to be mature osteoclasts, in comparison to WT BMMs (Figure 2B). Moreover, *Tmem64*$^{-/-}$ BMMs showed impaired osteoclast generation whether they were co-cultured with WT or *Tmem64*$^{-/-}$ osteoblasts (Figure S1D), and independent of RANKL expression levels (Figure S2E). These results strongly suggest that Tmem64 expression in osteoclast lineages is required for proper osteoclast differentiation. We also revealed that levels of *NFATc1*, *OSCAR*, *ctsk* and *ppargc1b*, which are markers of differentiated osteoclasts, were significantly lower in *Tmem64*$^{-/-}$ cells (Figure 2C), whereas neither expression of c-fms nor RANK, was altered in *Tmem64*$^{-/-}$ cells (Figure S3A). The proportion of osteoclast precursor cells (c-Fms^{+}c-Kit^{+}Mac-1^{low}) to the total number of bone marrow cells was equivalent in WT and *Tmem64*$^{-/-}$ mice (Figure 2D). Proliferation and apoptosis of osteoclasts *in vitro* in WT and *Tmem64*$^{-/-}$ cells were also comparable (Figure 2E and 2F). In addition, when cultured on dentine slices, the pit area formed from *Tmem64*$^{-/-}$ BMMs was small, but no difference in the pit area per osteoclast size was observed (Figure 2G). These results suggest that *Tmem64* is a crucial regulator of osteoclast differentiation; its absence reduced the number of mature osteoclasts, while their bone-resorption activity did not appear to be affected.

Deletion of *Tmem64* exacerbates RANKL-dependent Ca^{2+} oscillation and mitochondrial ROS generation

We next investigated the role of *Tmem64* in the regulation of RANKL-dependent signaling pathways, including ERK, p38, JNK, NF-κB, and AKT, which are activated via the RANKL-TRAF6-dependent axis (Kim et al., 2009). As shown in Figure 3A, there was no significant difference in RANKL-dependent activation between WT and *Tmem64*$^{-/-}$ BMMs. Moreover, activation of the M-CSF-stimulated signaling pathways was also unchanged (Figure S3B). In contrast, expression levels of c-fos and NFATc1—key regulators of osteoclast differentiation—were decreased during osteoclast formation in *Tmem64*$^{-/-}$ BMMs (Figure 3B). CREB phosphorylation by RANKL was significantly suppressed in *Tmem64*$^{-/-}$ BMMs without a substantial change in protein expression (Figure 3B). As previously reported (Sato et al., 2006), CREB is critical for RANKL-stimulated NFATc1 and c-fos induction in osteoclast precursors. To investigate whether enforced expression of CREB could rescue osteoclast formation in *Tmem64*$^{-/-}$ BMMs, we used retroviruses to introduce CREB or a dominant-negative inhibitor of CREB (A-CREB) into

WT or *Tmem64*$^{-/-}$ BMMs. When CREB was introduced the cells underwent normal osteoclast differentiation accompanied by significant induction of NFATc1 and c-fos (data not shown), whereas introduction of A-CREB led to strong suppression of osteoclast differentiation by RANKL (Figure 3C). These results indicate that *Tmem64* is required for RANKL-mediated CREB activation during osteoclastogenesis.

RANKL-RANK signaling activates phospholipase Cγ2 (PLCγ2) and leads to an increase in $[Ca^{2+}]_i$ via ITAM-harboring molecules DAP12 and FcRγ, followed by activation of CaMKIV, which mainly contributes to activation of CREB (Sato et al., 2006; Takayanagi, 2007a; Wada et al., 2006). We examined whether Tmem64 affects PLCγ2 activation by RANKL stimulation (Figure 3D, upper panel), and found no differences between WT and *Tmem64*$^{-/-}$ activation of PLCγ2 in BMMs, whereas CaMKIV was barely activated in RANKL-stimulated *Tmem64*$^{-/-}$ BMMs (Figure 3D, lower panel). Based on these data indicating that *Tmem64* regulates CaMKIV activation, we examined RANKL-induced $[Ca^{2+}]_i$ oscillation, which is important for CaMKIV activation (Sato et al., 2006). As shown in Figure 3E, RANKL-induced $[Ca^{2+}]_i$ oscillation was impaired in BMMs derived from *Tmem64*$^{-/-}$ mice.

Since mitochondrial ROS produced downstream of RANK and ITAM during osteoclastogenesis activate CREB (Ishii et al., 2009), we investigated whether ablation of *Tmem64* affected the production of mitochondrial ROS by RANKL. Using a mitochondrial ROS-specific dye (MitoSOX), we showed that the production of mitochondrial ROS was substantially inhibited in the absence of *Tmem64* after stimulation by RANKL for 6 hours (Figure 3F). Consistent with these data, PGC1β upregulation, which follows mitochondrial ROS production and CREB activation, was suppressed (Figure 3B) (Ishii et al., 2009). In order to verify the role of Tmem64, we infected *Tmem64*$^{-/-}$ BMMs with retroviral Tmem64 (MSCV-Tmem64). As expected, Ca^{2+} oscillation and mitochondrial ROS production were dramatically enhanced by RANKL stimulation (Figures 3G and 3H); transduced cells differentiated into mature osteoclasts (Figure S7B). Thus, *Tmem64* is required for proper $[Ca^{2+}]_i$ oscillation and optimal production of mitochondrial ROS induced by RANKL during osteoclast differentiation.

Tmem64 associates with SERCA2

When transfected into HEK293 cells, Tmem64 was mostly associated with microsomal fractions containing endoplasmic reticulum (data not shown). Therefore, to further investigate the molecular mechanism of Tmem64, we immunoprecipitated the microsomal fraction of HEK293T cells transfected with Flag-tagged Tmem64 and identified the associated proteins by Coomassie Blue staining followed by mass spectrometry (Figure S4 and Table S1). Interestingly, Tmem64 associated with SERCA2, a protein essential for spiking Ca^{2+} oscillations (Muller et al., 2006). To specifically determine the SERCA subtype that mediated osteoclast differentiation, we performed real-time PCR. As shown in Figure 4A, *Atp2a2* (encoding SERCA2) was strongly induced in comparison *Atp2a3* (encoding SERCA3), whereas *Atp2a1* (encoding SERCA1) was not detected and there was no difference in the expression of *Atp2a2* and *Atp2a3* between *Tmem64*$^{-/-}$ and WT cells. Immunoblotting of total proteins from RANKL+M-CSF-treated cells with an antibody specific for SERCA2 revealed that it was highly upregulated during osteoclast differentiation (Figure 4B). To confirm the association between Tmem64 and SERCA2, we co-transfected Myc-tagged SERCA2 and Flag-tagged Tmem64 into HEK293T cells. Co-immunoprecipitation (Co-IP) showed that Tmem64 and SERCA2 were strongly associated (Figure 4C). We then performed co-immunolabeling and confocal microscopy to clarify the subcellular localization of Tmem64 in HEK293T cells (Figure 4D). Confocal images indicated that Tmem64 co-localizes with SERCA2 in the ER; calreticulin was used as an ER marker. When retroviral Flag-tagged Tmem64 was reintroduced into *Tmem64*$^{-/-}$ BMMs,

we found that endogenous SERCA2 co-precipitated with Tmem64-Flag from Tmem64-complemented BMMs (Figure 4E). SERCA2 is a critical regulator of RANKL-induced osteoclast formation by RANKL-mediated $[Ca^{2+}]_i$ oscillations in the NFATc1 pathway (Yang et al., 2009), raising the possibility that suppression of SERCA2 activity may contribute to the phosphorylation of CREB by RANKL. Thus, we examined whether suppression of CREB phosphorylation impaired $[Ca^{2+}]_i$ oscillations in SERCA2 heterozygotes ($SERCA2^{+/-}$). As shown in Figure 4F, CREB activation was severely inhibited in $SERCA2^{+/-}$; we also observed that osteoclast differentiation was completely rescued by retroviral expression of CREB (Figure 4G). Consistent with these data, the production of mitochondrial ROS 6 hours after RANKL stimulation was suppressed in $SERCA2^{+/-}$ cells (Figure 4H, left panel). We also confirmed that *Tmem64* siRNA repressed the generation of mitochondrial ROS in SERCA2 WT cells (Figure 4H, right panel) and conversely, the retroviral expression of *Tmem64* rescued osteoclast differentiation in $SERCA2^{+/-}$ cells (Figure 4I). These data indicate that Tmem64 interaction with SERCA2 is critical in the Ca^{2+} signaling cascade for RANKL-induced CREB activation and mitochondrial ROS generation.

Tmem64 modulates SERCA2 activity by association with its regulatory C-terminal region during osteoclastogenesis

To gain insight into the SERCA activity critical for Ca^{2+} signaling modulation by Tmem64, we measured intrinsic Ca^{2+}-ATPase activity, which represents SERCA activity (Randriamboavonjy et al., 2008), in BMMs from WT and *Tmem64*$^{-/-}$ mice using an enzyme-coupled assay. As shown in Figure 5A, Ca^{2+}-ATPase activity was reduced by approximately 60% in *Tmem64*$^{-/-}$ BMMs versus WT BMMs. Ionomycin, an intracellular calcium-elevating compound, stimulates calcineurin/NFATc1 signal transduction in BMMs, which leads to enhanced osteoclast differentiation. These data indicate that both ER Ca^{2+} release and re-uptake by ER-process proteins, such as IP_3Rs and SERCA, are critically important to the Ca^{2+} signaling cascade. Consequently, decreased Ca^{2+} concentrations in the ER trigger activation of the store-operated Ca^{2+} entry (SOCE) pathway, thus activating SERCA in the ER (Takayanagi, 2007b), but it was unclear whether this occurred through increased activation or conductance of Ca^{2+} release channels, or from enhanced store filling. To clarify the mechanism of activation, we examined whether functional coordination of Ca^{2+} release and sequestration is required for RANKL-dependent osteoclastogenesis. We used a loss-of-function approach for SERCA2, employing thapsigargin, a specific inhibitor of SERCA. As shown in Figure 5B, ionomycin-induced intracellular Ca^{2+} influx synergistically enhanced $TRAP^+$ MNC formation induced by RANKL; and this effect was completely abolished by thapsigargin in WT cells without cytotoxicity (Figure S5A). In addition, ionomycin did not fully restore the osteoclast differentiation defects in the absence of Tmem64. Thus, modulation of SERCA2 activity by Tmem64 (and subsequent calcium uptake) is necessary for the RANKL-induced osteoclast differentiation.

One remaining question was how Tmem64 regulates SERCA2 activity. One possible mechanism is through a direct interaction with the regulatory region of SERCA2. The Camacho group demonstrated that the intraluminal loop (L7–8) domain of SERCA2 plays a critical role in the regulation of ER Ca^{2+} homeostasis in *Xenopus* oocytes (Li and Camacho, 2004). Overexpression of ERp57 specifically inhibits SERCA2 activity through association with the L7–8 domain of SERCA2. Based on this observation, we hypothesized that Tmem64 binds and/or modulates the L7–8 domain of SERCA2, which switches SERCA2 to its active form. To investigate this hypothesis, we generated deletion mutants of SERCA2 (Figure 5C) and looked for binding to Tmem64. As shown in Figure 5D, in vitro deletion mapping indicated that Tmem64 binds directly to the 257 amino acid C-terminal segment of SERCA2, which contains the L7–8 domain (SERCA2F2). Immunoprecipitation experiments

confirmed that SERCA2F1 (1–787), which lacks the C-terminal segment, did not bind to Tmem64-Flag. Further evaluation of the specificity of the Tmem64-SERCA2 association was addressed in competition assays using ERp57, which is moderately expressed during osteoclast differentiation without substantial changes in *Tmem64*$^{-/-}$ versus WT cells (Figure S5B). We confirmed the association between the SERCA2 C-terminus region and ERp57 (Figure S5C). As shown in Figure 5E, reciprocal co-immunoprecipitation performed using Tmem64-Flag and SERCA2-Myc, in addition to increasing the amount of ERp57-HA, demonstrated association between Tmem64 and SERCA2 is reduced by ERp57 in a dose-dependent manner, and that Tmem64 association with the L7–8 domain in the C-terminus region of SERCA2 was required for SERCA2 Ca^{2+} pump activation. Consistently, we also showed that ERp57 inhibited CREB phosphorylation and suppressed osteoclast differentiation (Figure S5D and S5E). Finally, to explore the relevance of our results to the modulation of SERCA2 activity, we examined whether Tmem64 is required for SERCA2 activation. As shown in Figure 5F, the activity of Ca^{2+}-ATPase was fully recovered in MSCV-Tmem64-introduced *Tmem64*$^{-/-}$ BMMs. Taken together, the results demonstrate that Tmem64 is required as a modulator of SERCA2 activity and mediates RANKL-dependent Ca^{2+} signaling during osteoclast differentiation.

DISCUSSION

Osteoclasts are highly specialized, multinucleated cells that tightly regulate skeletal homeostasis. They are differentiated from hematopoietic stem cells by macrophage colony-stimulating factor (M-CSF, also known as *Csf1*), which stimulates the proliferation and survival of osteoclast precursor cells and RANKL (also known as TNFSF11), a key cytokine for osteoclastogenesis and a member of the tumor necrosis factor (TNF) family. Recent studies have determined the function of NFATc1, which is induced by RANKL and plays a crucial role in differentiation, fusion, maturation, activation, and survival of osteoclasts (Ferron et al., 2011; Kim et al., 2008; Takayanagi, 2007b; Takayanagi et al., 2002). Transcription of NFATc1 is mainly regulated by Ca^{2+} signals, which are activated by co-stimulatory signaling via FcRγ and DAP12. Although the mechanism has not been clearly elucidated in osteoclasts, Ca^{2+} oscillation induced by RANKL is thought to be important for efficient activation of NFATc1 via the Ca^{2+}-dependent phosphatase calcineurin, which lies downstream of FcRγ and DAP12. After Ca^{2+} stimulation, activated NFATc1 has a short half-life. Thus, a “cycling hit” such as continuous Ca^{2+} spiking is required for long-lasting transcriptional activation of NFATc1 during osteoclastogenesis (Negishi-Koga and Takayanagi, 2009; Yang and Li, 2007). A Ca^{2+} cycling hit requires tight regulation of the reduction and refilling of ER Ca^{2+} stores. IP_3-mediated signaling has an IP_3R2- and IP_3R3-dependent physiological role in ER Ca^{2+} release during osteoclast differentiation (Kuroda et al., 2008). Recently, it has been reported to regulate Ca^{2+} entry processes during osteoclastogenesis by plasma membrane-localized Ca^{2+}-permeable channels, such as Orai1 and TRPV4 (Masuyama et al., 2008; Robinson et al., 2012). However, the mechanisms or molecules involved in Ca^{2+} re-uptake into ER stores by RANKL-dependent Ca^{2+} signaling are largely unknown. Here, we determined that ablation of Tmem64 impaired osteoclast differentiation, causing strong suppression of RANKL-triggered CREB activation and c-fos and NFATc1 induction. Further, *Tmem64*$^{-/-}$ BMMs exhibited attenuated RANKL-induced Ca^{2+} oscillations. Consistent with these data, introduction of CREB, c-fos, or Tmem64 into *Tmem64*$^{-/-}$ BMMs were sufficient to rescue osteoclastogenesis (Figures 3C and S7).

Tmem64 has seven predicted transmembrane domains and a conserved SNARE domain by TMPRED program analysis, but its function has been completely unknown. In this study, we showed that Tmem64 is associated mainly with ER. Intriguingly, in vitro pull-down assays and co-immunoprecipitation analyses revealed that Tmem64 associates with SERCA2, which impairs Ca^{2+} oscillations and leads to defective osteoclast differentiation in

heterozygotes. Furthermore, we provide mechanistic clarification of both the suppression of CREB phosphorylation and the down-regulation of NFATc1 during osteoclastogenesis (Figure 4F). Indeed, we observed decreased SERCA2 activity (by about 60%) in *Tmem64*$^{-/-}$ BMMs compared with WT cells. However, it is not known how SERCA2 regulates intracellular Ca^{2+} homeostasis for Ca^{2+} oscillations during osteoclastogenesis. We found that Tmem64 specifically associated with the L7–8 domain of SERCA2 (SERCA2F2) by competing with ERp57, which is necessary for Ca^{2+} oscillations, whereas Tmem64 is required for their activation. Post-translational modifications, such as SUMOylation, are critical regulators of protein function and play an important role in various cellular processes (Geiss-Friedlander and Melchior, 2007). Kho et al. determined that SERCA2a function is regulated by SUMO1-dependent modulation in heart failure (Kho et al., 2011). SUMOylation of SERCA2a elevated its stability and activity, thereby improving heart function. We also identified E3 SUMO-protein ligase RanBP2 as a Tmem64-associated factor via co-immunoprecipitation (Table S1). RanBP2 binds Ubc9 and SUMO1 and enhances SUMOylation of HDAC4, Sp100, and PML (Kirsh et al., 2002; Wilkinson and Henley, 2010); however, the relationship between Tmem64, SERCA2 and RanBP2 requires further investigation.

One of the most noteworthy findings of this study is that RANKL-induced Ca^{2+} signaling is dependent on SERCA2 activity, which is critically mediated by Tmem64. Our study provides important insight into the coordinated mechanism of SOCE and Ca^{2+} release-activated Ca^{2+} (CRAC) channels in osteoclasts. Furthermore, significant suppression of SERCA2 activity by RANKL correlated with the generation of mitochondrial ROS. Involvement of mitochondrial ROS in NFATc1 induction has been clearly demonstrated (Ishii et al., 2009; Ke et al., 2006). However, these data are subject to different interpretations with respect to the cause-effect relationship between Ca^{2+} signaling and mitochondrial ROS generation by RANKL. Our study shows that Ca^{2+} oscillations lead to the production of mitochondrial ROS, which is reversed by full-length Tmem64 (Figures 3G and 3H).

Interestingly we also showed that cyclosporin A treatment significantly inhibited RANKL-induced Tmem64 mRNA expression (Figure S3C), suggesting that NFATc1 is mediating the upregulation of Tmem64 mRNA expression during osteoclast differentiation. Taken together with its importance to Ca^{2+} oscillation/NFATc1 activation, *Tmem64* is likely to control the positive feedback controlled regulation of NFATc1-mediated osteoclastogenesis.

Although not studied in detail here, the effect of *Tmem64* on osteoblasts appears to be cell-intrinsic, as shown in calvarial or bone marrow stromal cells cultured in osteogenic media. However, the detailed mechanism of how Tmem64 regulates osteoblast differentiation needs future study. Moreover, although we clearly showed that there was decreased osteoclast activity and increased osteoblast activity in *Tmem64*$^{-/-}$ mice, and Tmem64 has a cell-intrinsic role in both cell types, it is not clear in which cell type Tmem64 is more important to the Tmem64$^{-/-}$ bone volume phenotype. This will require future studies involving cell-type specific deletion of Tmem64.

In summary, our study suggests that Tmem64 in the ER of BMMs contributes to the efficient activation of SERCA2 (Figure 6). Impairment of Ca^{2+} signaling pathways in the absence of Tmem64 reduces SERCA2 activity and mitochondrial ROS production, resulting in inefficient osteoclast differentiation and function. Identification and elucidation of key mediators of Ca^{2+} oscillation by RANKL should aid in the development of therapeutic strategies for the treatment of skeletal diseases.

EXPERIMENTAL PROCEDURES

Animals and materials

For *Tmem64*-deficient mice, a mouse embryonic stem cell line (SYA242, stain 129P2/OlaHsd) with an insertional mutation in Tmem64 was obtained from BayGenomics (Stryke et al., 2003) through the International Gene Trap Consortium (Nord et al., 2006; Skarnes et al., 2004). The gene-trapping vector, pGT01xf, was designed to introduce an in-frame fusion between the 5′ exons of the trapped gene and a reporter, β-geo (a fusion of β-galactosidase and neomycin phosphotransferase II). To determine the location of the genomic insertion site in the SYA242 stem cell line, genomic DNA was extracted from the embryonic stem cells by using the DNeasy blood and tissue kit (Qiagen). PCR was then performed using primers P1 (within intron 2–3 of Tmem64, 5′-AGTCCATCGCGCTCAAGTGG-3′) and P3 (within the β–geo gene of the gene-trapping vector, 5′-AGTATCGGCCTCAGGAAGATCG-3′), and the PCR product was sequenced to verify the insertion site. The embryonic stem cells were injected into C57BL/6 blastocysts to create chimeric mice, which were bred with C57BL/6 mice to generate heterozygous *Tmem64*-deficient mice. The heterozygous mice were interbred to generate all Tmem64-deficient genotypes. Primers: P1, P2 (5′-GCATGCACTGTAGACCAGGTGC-3′) and P3 were used for multiplex genotyping thereof all 3 genotypes (+/+, +/−, −/−). The generation of SERCA2$^{+/-}$ mice was previously reported by our group (Prasad et al., 2005). We used 6~8-week-old male mice and all animal work performed with veterinary supervision in an accredited facility using protocols approved by the Animal Care and Use Committee of the University of Pennsylvania. All other reagents were acquired from Sigma.

Micro–computed tomography, histological analysis, measurement of mineral deposition rate

Micro-computed tomography, histological analysis, and measurement of mineral deposition rate were performed as previously described; for details, see the supplementary data (Lee et al., 2006).

Osteoclast differentiation

Bone marrow-derived macrophages (BMMs) were obtained from cultures of bone marrow collected from 6-8-week-old male tibia and femur as described (Song et al., 2012). Cells were cultured for 3 days in α-MEM containing M-CSF (60 ng/ml) and RANKL (150 ng/ml). After culture for 3 days, the cells were fixed with 3.7% formaldehyde in PBS for 10 min and stained for TRAP using the Acid Phosphatase, Leukocyte (TRAP) kit (Sigma). TRAP-positive multinucleated cells containing 3 or more nuclei and an actin ring were counted. To analyze bone pit formation, BMMs (1×10^4 cells/well in 96-well plates) were seeded onto dentine slices and allowed to differentiate into osteoclasts in the presence of M-CSF and RANKL for 5 days, with a change of medium after 2 days. Cells on the dentin slice were removed by washing with PBS, and stained with 1% toluidine blue (Sigma-Aldrich); pit formation was analyzed using the VIA-160 video image-maker measurement system (Boeckeler Instruments).

Osteoclast proliferation and apoptosis assay

Proliferation was measured by absorbance at 450 nm by using the BrdU Cell Proliferation Assay Kit (Cell Signaling) according to the manufacturer's protocol. Osteoclast apoptosis was assayed as previously described (Kim et al., 2009). Briefly, purified osteoclasts were cultured without RANKL for 9 hr and then measured with a caspase-3 colorimetric assay kit (R&D Systems).

Mitochondrial ROS measurement

ROS were measured by flow cytometry using the MitoSOX™ Red mitochondrial superoxide indicator. Cells were treated as indicated, stained with 5 μM MitoSOX™ Red for 10 min, and washed with media 3 times for 2 min per wash. Cells were detached with Enzyme-Free Cell Dissociation Solution (Millipore, Bedford, MA). Detached cells were washed once with PBS and resuspended in PBS containing 2% FBS and 0.7 mM EDTA (disodium salt). Fluorescence was recorded on the PE channel (excitation 510 nm, emission 580 nm) of a FACSCalibur (BD Biosciences, Heidelberg, Germany). For each analysis, 1×10^4 cells were counted. Mean values of the log fluorescence in individual samples were recorded and normalized to control cells.

SERCA2 activity

SERCA2 activity was measured with an enzyme-coupled assay according to previously described methods (Randriamboavonjy et al., 2008).

$[Ca^{2+}]_i$ oscillation

A total of 5×10^4 BMM cells were seeded on the cover slips in the bottom of a 24-well plate and cultured with RANKL (150 ng/ml) in the presence of M-CSF (60 ng/ml) for 48 hr. Cells were then incubated in the presence of 5 μM fluo-4 AM, 10 μM Fura Red AM, and 0.05% pluronic F-127 (Invitrogen) for 30 min in serum and phenol red-free α-MEM (Invitrogen). Cells were washed twice with α-MEM and post-incubated in α-MEM with 10% FBS, and 10 ng/ml RANKL for 20 min. The dye-loaded cells were washed twice with α-MEM and Hank's buffered salt solution (HBSS). Cells were viewed on the inverted stage of a confocal microscope (Leica). The loading medium consisted of 115 mM NaCl, 20 mM HEPES-NaOH, 5.4 mM KCl, 1 mM $MgCl_2$, 2 mM $CaCl_2$, and 10 mM glucose (pH 7.4). At an excitation wavelength of 488 nm, emission at 493–539 nm for fluo-4 and 653–742 nm for Fura Red was analyzed simultaneously at 5 s intervals. The ratio of fluo-4 to Fura Red was calculated to estimate intracellular Ca^{2+} influx concentrations in single cells (Sato et al., 2006).

Statistical analysis

Data were analyzed be using Student's 2-tailed *t*-test and are presented as means ± SEMs or ± SDs, as indicated. Means were checked for statistical differences using the Student's *t* test with error probabilities of $*P < 0.01$ and $**P < 0.05$.

Supplementary Material

Refer to Web version on PubMed Central for supplementary material.

Acknowledgments

We are thankful to Dr. Daewon Jeong (Youngnam University, Korea) and Dr. Matthew C. Walsh (University of Pennsylvania) for helpful discussions, for critical reading of the manuscript. This work was in part supported by the Korea Institute or Oriental Medicine (KIOM) from Ministry of Education, Science and Technology (MEST) (No. K12050 to T.K., Y.C.), an AHA Beginning Grant-in-Aid award (No. 11BGIA7720005 to V.P.), the National Research Foundation of Korea (NRF) Grant funded by the Korea government (MEST) (No. 2011-0030719 to S.H.L.) and by NIH (to Y.C.)

References

Arvanitis DA, Vafiadaki E, Fan GC, Mitton BA, Gregory KN, Del Monte F, Kontrogianni-Konstantopoulos A, Sanoudou D, Kranias EG. Histidine-rich Ca-binding protein interacts with

sarcoplasmic reticulum Ca-ATPase. Am. J. Physiol. Heart Circ. Physiol. 2007; 293:H1581–1589. [PubMed: 17526652]

Dally S, Bredoux R, Corvazier E, Andersen JP, Clausen JD, Dode L, Fanchaouy M, Gelebart P, Monceau V, Del Monte F, et al. Ca2+-ATPases in non-failing and failing heart: evidence for a novel cardiac sarco/endoplasmic reticulum Ca2+-ATPase 2 isoform (SERCA2c). Biochem. J. 2006; 395:249–258. [PubMed: 16402920]

Ferron M, Boudiffa M, Arsenault M, Rached M, Pata M, Giroux S, Elfassihi L, Kisseleva M, Majerus PW, Rousseau F, et al. Inositol polyphosphate 4-phosphatase B as a regulator of bone mass in mice and humans. Cell Metab. 2011; 14:466–477. [PubMed: 21982707]

Feske S. Calcium signalling in lymphocyte activation and disease. Nat. Rev. Immunol. 2007; 7:690–702. [PubMed: 17703229]

Fu S, Yang L, Li P, Hofmann O, Dicker L, Hide W, Lin X, Watkins SM, Ivanov AR, Hotamisligil GS. Aberrant lipid metabolism disrupts calcium homeostasis causing liver endoplasmic reticulum stress in obesity. Nature. 2011; 473:528–531. [PubMed: 21532591]

Geiss-Friedlander R, Melchior F. Concepts in sumoylation: a decade on. Nat. Rev. Mol. Cell Biol. 2007; 8:947–956. [PubMed: 18000527]

Ishii KA, Fumoto T, Iwai K, Takeshita S, Ito M, Shimohata N, Aburatani H, Taketani S, Lelliott CJ, Vidal-Puig A, et al. Coordination of PGC-1beta and iron uptake in mitochondrial biogenesis and osteoclast activation. Nat. Med. 2009; 15:259–266. [PubMed: 19252502]

John LM, Lechleiter JD, Camacho P. Differential modulation of SERCA2 isoforms by calreticulin. J. Cell Biol. 1998; 142:963–973. [PubMed: 9722609]

Karsenty G, Wagner EF. Reaching a genetic and molecular understanding of skeletal development. Dev. Cell. 2002; 2:389–406. [PubMed: 11970890]

Ke Q, Li J, Ding J, Ding M, Wang L, Liu B, Costa M, Huang C. Essential role of ROS-mediated NFAT activation in TNF-alpha induction by crystalline silica exposure. Am. J. Physiol. Lung Cell. Mol. Physiol. 2006; 291:L257–264. [PubMed: 16489119]

Kho C, Lee A, Jeong D, Oh JG, Chaanine AH, Kizana E, Park WJ, Hajjar RJ. SUMO1-dependent modulation of SERCA2a in heart failure. Nature. 2011; 477:601–605. [PubMed: 21900893]

Kim H, Choi HK, Shin JH, Kim KH, Huh JY, Lee SA, Ko CY, Kim HS, Shin HI, Lee HJ, et al. Selective inhibition of RANK blocks osteoclast maturation and function and prevents bone loss in mice. J. Clin. Invest. 2009; 119:813–825. [PubMed: 19258703]

Kim K, Lee SH, Ha Kim J, Choi Y, Kim N. NFATc1 induces osteoclast fusion via up-regulation of Atp6v0d2 and the dendritic cell-specific transmembrane protein (DC-STAMP). Mol. Endocrinol. 2008; 22:176–185. [PubMed: 17885208]

Kim N, Takami M, Rho J, Josien R, Choi Y. A novel member of the leukocyte receptor complex regulates osteoclast differentiation. J. Exp. Med. 2002; 195:201–209. [PubMed: 11805147]

Kirsh O, Seeler JS, Pichler A, Gast A, Muller S, Miska E, Mathieu M, Harel-Bellan A, Kouzarides T, Melchior F, et al. The SUMO E3 ligase RanBP2 promotes modification of the HDAC4 deacetylase. EMBO J. 2002; 21:2682–2691. [PubMed: 12032081]

Koga T, Inui M, Inoue K, Kim S, Suematsu A, Kobayashi E, Iwata T, Ohnishi H, Matozaki T, Kodama T, et al. Costimulatory signals mediated by the ITAM motif cooperate with RANKL for bone homeostasis. Nature. 2004; 428:758–763. [PubMed: 15085135]

Kuroda Y, Hisatsune C, Nakamura T, Matsuo K, Mikoshiba K. Osteoblasts induce Ca2+ oscillation-independent NFATc1 activation during osteoclastogenesis. Proc. Natl. Acad. Sci. USA. 2008; 105:8643–8648. [PubMed: 18552177]

Lee SH, Rho J, Jeong D, Sul JY, Kim T, Kim N, Kang JS, Miyamoto T, Suda T, Lee SK, et al. v-ATPase V0 subunit d2-deficient mice exhibit impaired osteoclast fusion and increased bone formation. Nat. Med. 2006; 12:1403–1409. [PubMed: 17128270]

Li Y, Camacho P. Ca2+-dependent redox modulation of SERCA 2b by ERp57. J. Cell Biol. 2004; 164:35–46. [PubMed: 14699087]

Masuyama R, Vriens J, Voets T, Karashima Y, Owsianik G, Vennekens R, Lieben L, Torrekens S, Moermans K, Vanden Bosch A, et al. TRPV4-mediated calcium influx regulates terminal differentiation of osteoclasts. Cell Metab. 2008; 8:257–265. [PubMed: 18762026]

Muller EJ, Caldelari R, Kolly C, Williamson L, Baumann D, Richard G, Jensen P, Girling P, Delprincipe F, Wyder M, et al. Consequences of depleted SERCA2-gated calcium stores in the skin. J. Invest. Dermatol. 2006; 126:721–731. [PubMed: 16397524]

Negishi-Koga T, Takayanagi H. Ca2+-NFATc1 signaling is an essential axis of osteoclast differentiation. Immunol. Rev. 2009; 231:241–256. [PubMed: 19754901]

Nord AS, Chang PJ, Conklin BR, Cox AV, Harper CA, Hicks GG, Huang CC, Johns SJ, Kawamoto M, Liu S, et al. The International Gene Trap Consortium Website: a portal to all publicly available gene trap cell lines in mouse. Nucleic Acids Res. 2006; 34:D642–648. [PubMed: 16381950]

Prasad V, Boivin GP, Miller ML, Liu LH, Erwin CR, Warner BW, Shull GE. Haploinsufficiency of Atp2a2, encoding the sarco(endo)plasmic reticulum Ca2+-ATPase isoform 2 Ca2+ pump, predisposes mice to squamous cell tumors via a novel mode of cancer susceptibility. Cancer Res. 2005; 65:8655–8661. [PubMed: 16204033]

Randriamboavonjy V, Pistrosch F, Bolck B, Schwinger RH, Dixit M, Badenhoop K, Cohen RA, Busse R, Fleming I. Platelet sarcoplasmic endoplasmic reticulum Ca2+-ATPase and mu-calpain activity are altered in type 2 diabetes mellitus and restored by rosiglitazone. Circulation. 2008; 117:52–60. [PubMed: 18071073]

Robinson LJ, Mancarella S, Songsawad D, Tourkova IL, Barnett JB, Gill DL, Soboloff J, Blair HC. Gene disruption of the calcium channel Orai1 results in inhibition of osteoclast and osteoblast differentiation and impairs skeletal development. Lab. Invest. 2012; 92:1071–1083. [PubMed: 22546867]

Sahoo SK, Kim T, Kang GB, Lee JG, Eom SH, Kim do H. Characterization of calumenin-SERCA2 interaction in mouse cardiac sarcoplasmic reticulum. J. Biol. Chem. 2009; 284:31109–31121. [PubMed: 19740751]

Sato K, Suematsu A, Nakashima T, Takemoto-Kimura S, Aoki K, Morishita Y, Asahara H, Ohya K, Yamaguchi A, Takai T, et al. Regulation of osteoclast differentiation and function by the CaMK-CREB pathway. Nat. Med. 2006; 12:1410–1416. [PubMed: 17128269]

Shimura M, Minamisawa S, Takeshima H, Jiao Q, Bai Y, Umemura S, Ishikawa Y. Sarcalumenin alleviates stress-induced cardiac dysfunction by improving Ca2+ handling of the sarcoplasmic reticulum. Cardiovasc. Res. 2008; 77:362–370. [PubMed: 18006473]

Skarnes WC, von Melchner H, Wurst W, Hicks G, Nord AS, Cox T, Young SG, Ruiz P, Soriano P, Tessier-Lavigne M, et al. A public gene trap resource for mouse functional genomics. Nat. Genet. 2004; 36:543–544. [PubMed: 15167922]

Song H, Kim H, Lee K, Lee DH, Kim TS, Song JY, Lee D, Choi D, Ko CY, Kim HS, et al. Ablation of Rassf2 induces bone defects and subsequent haematopoietic anomalies in mice. EMBO J. 2012; 31:1147–1159. [PubMed: 22227519]

Stryke D, Kawamoto M, Huang CC, Johns SJ, King LA, Harper CA, Meng EC, Lee RE, Yee A, L'Italien L, et al. BayGenomics: a resource of insertional mutations in mouse embryonic stem cells. Nucleic Acids Res. 2003; 31:278–281. [PubMed: 12520002]

Takayanagi H. Osteoimmunology: shared mechanisms and crosstalk between the immune and bone systems. Nat. Rev. Immunol. 2007a; 7:292–304. [PubMed: 17380158]

Takayanagi H. The role of NFAT in osteoclast formation. Ann. N. Y. Acad. Sci. 2007b; 1116:227–237. [PubMed: 18083930]

Takayanagi H, Kim S, Koga T, Nishina H, Isshiki M, Yoshida H, Saiura A, Isobe M, Yokochi T, Inoue J, et al. Induction and activation of the transcription factor NFATc1 (NFAT2) integrate RANKL signaling in terminal differentiation of osteoclasts. Dev. Cell. 2002; 3:889–901. [PubMed: 12479813]

Teitelbaum SL, Ross FP. Genetic regulation of osteoclast development and function. Nat. Rev. Genet. 2003; 4:638–649. [PubMed: 12897775]

Wada T, Nakashima T, Hiroshi N, Penninger JM. RANKL-RANK signaling in osteoclastogenesis and bone disease. Trends Mol. Med. 2006; 12:17–25. [PubMed: 16356770]

Walsh MC, Kim N, Kadono Y, Rho J, Lee SY, Lorenzo J, Choi Y. Osteoimmunology: interplay between the immune system and bone metabolism. Annu. Rev. Immunol. 2006; 24:33–63. [PubMed: 16551243]

Wilkinson KA, Henley JM. Mechanisms, regulation and consequences of protein SUMOylation. Biochem. J. 2010; 428:133–145. [PubMed: 20462400]

Yang S, Li YP. RGS10-null mutation impairs osteoclast differentiation resulting from the loss of [Ca2+]i oscillation regulation. Genes Dev. 2007; 21:1803–1816. [PubMed: 17626792]

Yang YM, Kim MS, Son A, Hong JH, Kim KH, Seo JT, Lee SI, Shin DM. Alteration of RANKL-induced osteoclastogenesis in primary cultured osteoclasts from SERCA2+/− mice. J. Bone Miner. Res. 2009; 24:1763–1769. [PubMed: 19419309]

Zaidi M. Skeletal remodeling in health and disease. Nat. Med. 2007; 13:791–801. [PubMed: 17618270]

Zelzer E, Olsen BR. The genetic basis for skeletal diseases. Nature. 2003; 423:343–348. [PubMed: 12748653]

Highlights

- *Tmem64*-deficient mice show increased bone volume
- *Tmem64* deficiency reduces $[Ca^{2+}]_i$ oscillation in response to RANKL stimulation
- Tmem64 interacts with SERCA2
- Tmem64 positively regulates osteoclast formation via SERCA2/Ca^{2+} signaling

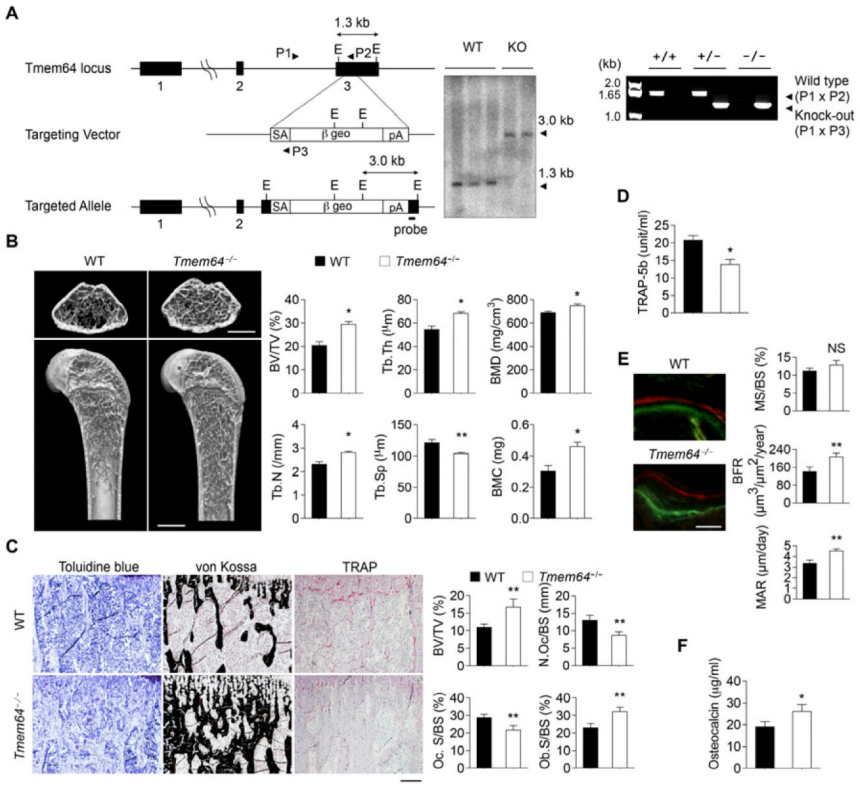

Figure 1. Ablation of *Tmem64* enhances bone density in mice

(A) Generation of *Tmem64* knockout mice (Left panel). E, EcoRI; TRAP cassette (Neo/β-galactosidase); SA, splice acceptor; pA, polyadenylation sequence. Homologous recombination was confirmed by Southern blot analysis of EcoRI-digested genomic DNA with a 3′ region probe (Middle panel). PCR genotyping analysis of $Tmem64^{+/+}$, $Tmem64^{+/-}$, *and* $Tmem64^{-/-}$ mice (Right panel). (B) Microcomputed tomography (μCT) images of the proximal femur from WT and $Tmem64^{-/-}$ mice (top, axial view of the metaphyseal region; bottom, longitudinal view). BV/TV, trabecular bone volume per tissue volume; Tb.Th, trabecular thickness; BMD, bone mineral density; Tb.N, trabecular number; Tb.Sp, trabecular spacing; BMC, bone mineral content. Scale bar, 1 mm. (C) Histological analysis of tibias from 8-week-old WT and $Tmem64^{-/-}$ mice. Tibial sections were stained with Toluidine blue (Left panels), von Kossa (Middle panels) or for TRAP (Right panels). N.Oc/BS, osteoclast number per bone surface; Oc.S/BS, osteoclast surface per bone surface; Ob.S/BS, osteoblast surface per bone surface; BV/TV, bone volume per tissue volume. Scale bar, 50 μm. (D) Serum TRAP-5b abundance in WT and $Tmem64^{-/-}$ mice. (E) Dynamic histomorphometry of tibia from 8-week-old WT and $Tmem64^{-/-}$ mice. MS/BS, mineralizing surface per bone surface; BFR, bone formation (per trabecular surface); MAR, mineral apposition rate. Scale bar, 10 μm. (F) Serum osteocalcin abundance in WT and $Tmem64^{-/-}$ mice. $*P < 0.01$, $**P < 0.05$ between the indicated groups. NS, not significant. Data are represented as mean ± SD.

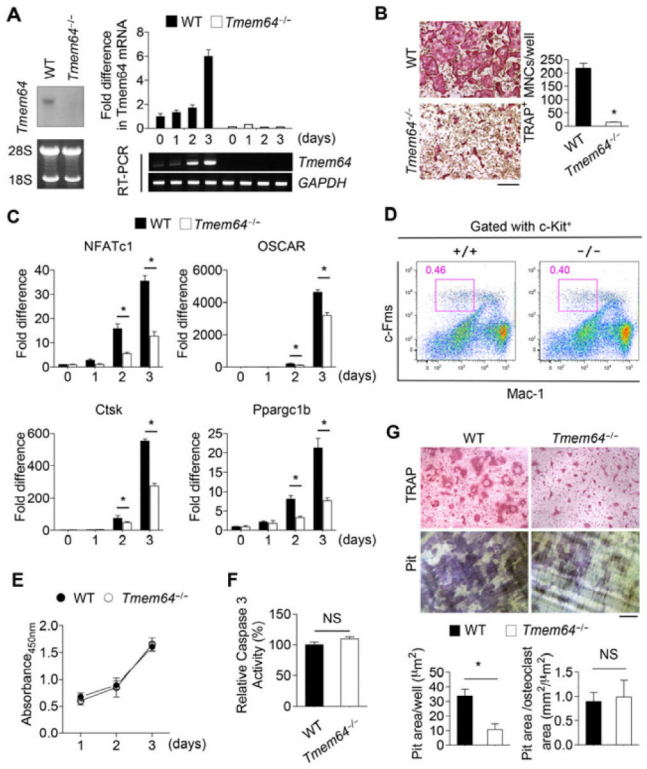

Figure 2. Tmem64 deficiency inhibited osteoclastogenesis and bone resorption

(A) Northern blot analysis of Tmem64 mRNA in BMMs from WT and *Tmem64*$^{-/-}$ mice (Left panel), and real-time PCR (Right upper) and conventional RT-PCR (Right lower) of *Tmem64* mRNA expression during osteoclast differentiation. (B) Osteoclast differentiation of the WT and *Tmem64*$^{-/-}$ cells. Right shows the number of TRAP^{+} MNCs. Scale bar, 100 μm. (C) Expression of osteoclast marker genes during osteoclastogenesis. Total RNA was collected on the indicated days and subjected to real-time PCR. (D) The percent frequency of a population of osteoclast precursor cells (c-Fms^{+}c-Kir^{+}Mac-1^{low}) is shown as the mean ± SD. (E) Proliferation was assessed by the absorbance of incorporated BrdU in WT and *Tmem64*$^{-/-}$ BMMs. (F) Caspase-3 activity was measured in mature osteoclasts. (G) Bone resorption activity of WT and *Tmem64*$^{-/-}$ osteoclast. After differentiation of BMMs into osteoclasts on dentine slices, cells were stained with the TRAP Kit and pit area was analyzed. Scale bar, 200 μm. *$P < 0.01$ between the indicated groups. NS, not significant. Data are represented as mean ± SD.

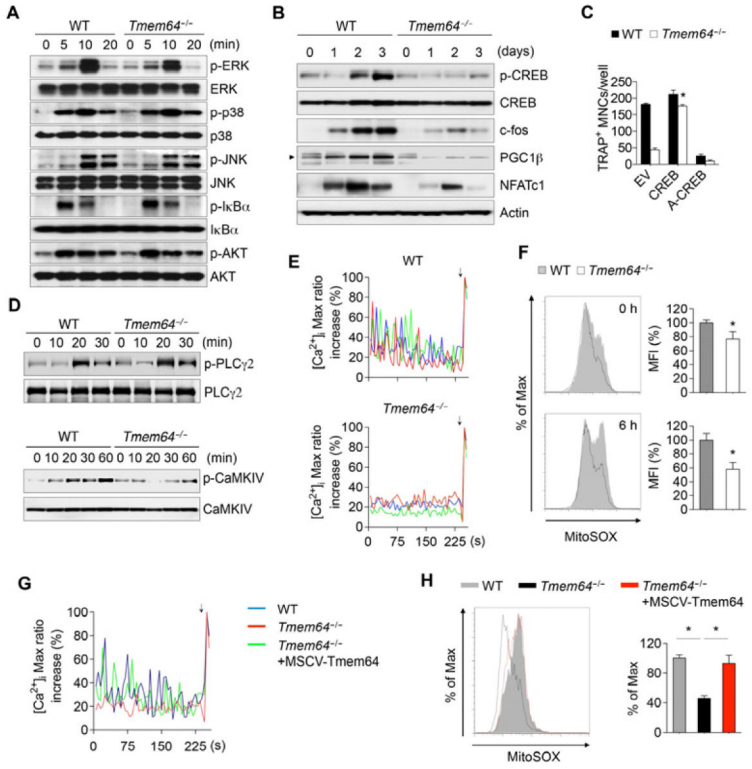

Figure 3. *Tmem64*-deficient BMMs inhibits RANKL-dependent Ca^{2+} oscillation and generation of mitochondrial ROS

(A) RANKL-induced ERK, p38, JNK, IκB and AKT phosphorylation in BMMs derived from WT and *Tmem64*$^{-/-}$ mice. (B) Activation of CREB and expression of c-fos, PGC1β (indicated with arrowhead) and NFATc1 during osteoclast differentiation. (C) Rescue of osteoclastogenesis in *Tmem64*$^{-/-}$ BMMs by CREB. Data are represented as mean ± SD. (D) RANKL-induced PLCγ2 and CaMKIV phosphorylation in WT and *Tmem64*$^{-/-}$ BMMs. (E) RANKL-induced oscillatory changes in $[Ca^{2+}]_i$ concentration. Addition of 10 μM ionomycin at the end of each experiment is indicated by an arrow. Each color indicates a different cell in the same field. (F) RANKL-mediated mitochondrial ROS production in BMMs from WT and *Tmem64*$^{-/-}$ mice. Data are expressed as relative MFI (%) ± SEM from 3 independent experiments and histograms show 1 representative experiment. (G) Retroviral Tmem64 introduction rescued RANKL-induced Ca^{2+} oscillations in *Tmem64*$^{-/-}$ BMMs. Cells from WT and *Tmem64*$^{-/-}$ mice were transduced with empty or MSCV-Tmem64 retrovirus and then subjected to Ca^{2+} oscillation. The addition of 10μM ionomycin at the end of each experiment is indicated by an arrow. (H) Retroviral Tmem64 rescued RANKL-induced mitochondrial ROS generation in *Tmem64*$^{-/-}$ BMMs. Cells from WT and *Tmem64*$^{-/-}$ mice were transduced with empty or MSCV-Tmem64 retrovirus and subjected to FACS analysis. Bar graph shows results of at least 3 independent experiments and histograms show 1 representative experiment. $*P < 0.01$ between the indicated groups.

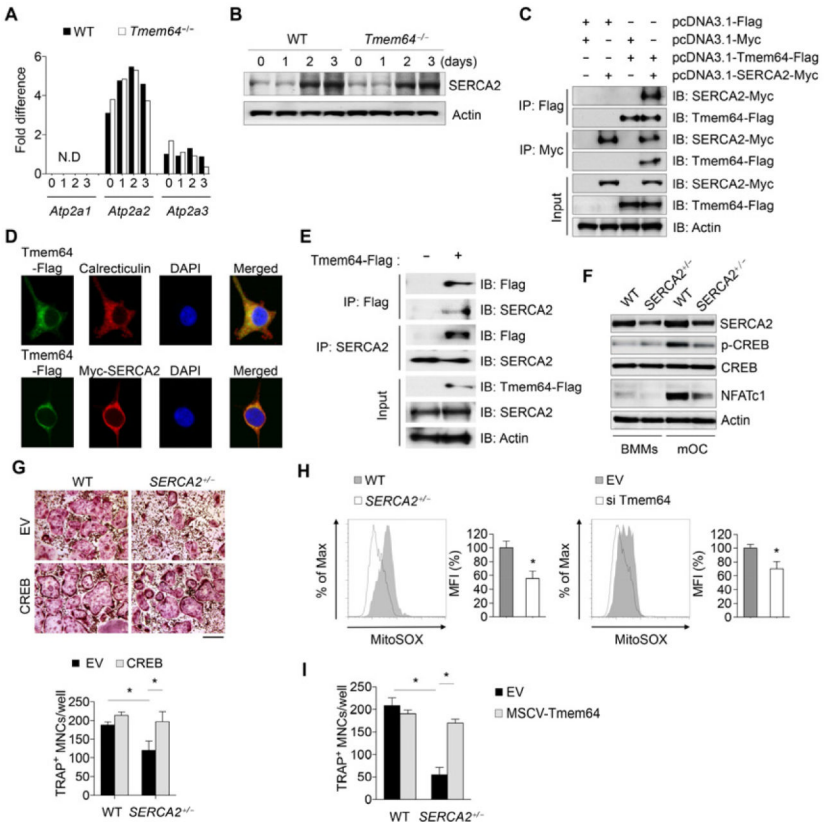

Figure 4. *Tmem64* modulates CREB phosphorylation and mitochondrial ROS generation through association with SERCA2

(A) Expression of SERCA isotypes during osteoclast differentiation. (B) Expression of SERCA2 during osteoclast differentiation in WT and *Tmem64*$^{-/-}$ BMMs. (C) Physical association between Tmem64 and SERCA2. HEK293T cells were transfected with indicated vectors. Flag or Myc immunoprecipitates were immunoblotted with anti-Flag or anti-Myc to visualize. (D) Immunohistochemistry of Tmem64 and SERCA2. HEK293T cells were cotransfected with Flag-Tmem64 and Myc-SERCA2, and calreticulin was used as an ER marker. (E) Tmem64$^{-/-}$ BMMs were transduced with the Flag-tagged Tmem64. Cell lysates were prepared and subjected to IP with anti-Flag or anti-SERCA2 antibodies, and immunoblotted with indicated antibodies. (F) Western blot analysis of phospho-CREB and NFATc1 expression in BMMs and osteoclasts. (G) Osteoclast differentiation rescued by retroviral expression of CREB in *SERCA2*$^{+/-}$ BMMs. Data are represented as mean ± SD. (H) RANKL-induced mitochondrial ROS generation in BMMs from WT and *SERCA2*$^{+/-}$ mice (left panel) and Tmem64 siRNA suppressed mitochondrial ROS production (right panel). Data are expressed as relative MFI (%) ± SEM from 3 independent experiments and histograms show 1 representative experiment. (I) Osteoclast differentiation rescued by retroviral expression of Tmem64 in *SERCA2*$^{+/-}$ BMMs. Data are represented as mean ± SD. *$P < 0.01$ between the indicated groups.

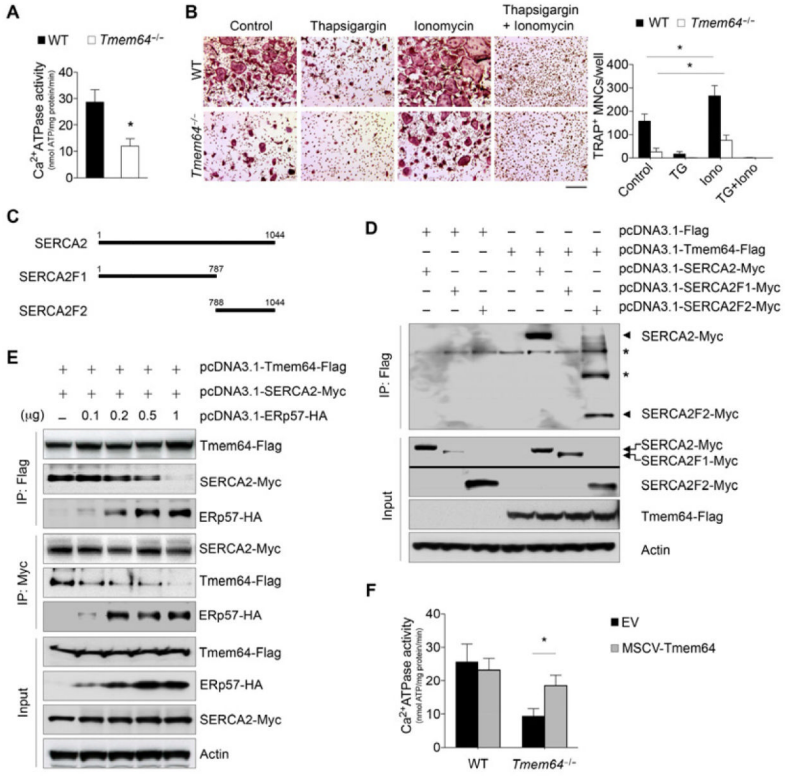

Figure 5. Tmem64 modulates RANKL-stimulated Ca^{2+} signal via interaction with SERCA2 C-terminus region

(A) Comparison of Ca^{2+}-ATPase activity from WT and *Tmem64*$^{-/-}$ BMMs. Details described in *Materials and methods*. (B) Induction of Ca^{2+} by ionomycin only partially rescued osteoclast differentiation of *Tmem64*$^{-/-}$ BMMs. BMMs were cultured with thapsigargin (5nM) and ionomycin (0.5μM) for 3 days with medium containing M-CSF and RANKL. (C) Schematic representation of SERCA2 and the series of SERCA2 deletion constructs. (D) Tmem64 interacts with the SERCA2 C-terminus. Flag-tagged Tmem64 coimmunoprecipitates with the Myc-tagged SERCA2 deletion series. HEK293T cells were transfected as indicated with Tmem64-Flag, SERCA2-Myc, SERCA2F1-Myc and SERCA2F2-Myc. Cells were lysed and Tmem64 was immunoprecipitated with anti-Flag antibody. Coimmunoprecipitated SERCA2 was detected by anti-Myc antibody. (E) Competitive interaction between Tmem64 and ERp57. HEK293T cells were transfected with a constant amount (1 μg) of pcDNA3.1-Tmem64-Flag and pcDNA3.1-SERCA2-Myc and increasing amounts (0, 0.1, 0.2, 0.5 and 1 μg) of pcDNA3.1-ERp57-HA; empty vector was added to ensure a similar amount of DNA was transfected in each sample. After 24 h, cell lysates were incubated with Flag and HA-affinity agarose gel beads and western blotted with the indicated antibodies. (F) Retroviral Tmem64 introduction rescued Ca^{2+}-ATPase activity in *Tmem64*$^{-/-}$ BMMs. $*P < 0.01$ between the indicated groups. Data are represented as mean ± SD.

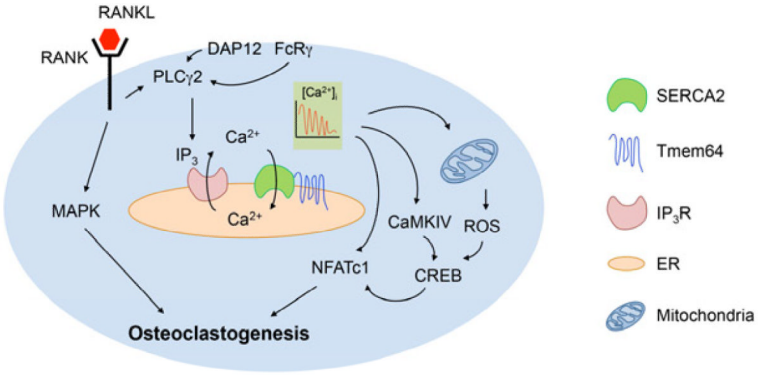

Figure 6. Schematic model depicting the role of *Tmem64*-mediated Ca^{2+} oscillation in production of mitochondrial ROS during OC differentiation

Shown are mechanisms that involve the RANKL-stimulated Ca^{2+} signal pathway. Association between Tmem64 and SERCA2 in the ER leads to cytosolic Ca^{2+} spiking for activation of NFATc1 and production of mitochondrial ROS, thereby triggering a Ca^{2+} signaling cascades that promote osteoclast differentiation and activation.